

Magnetic Coupled Circuits Modeling of Induction Machines Oriented to Diagnostics

Tarek AROUI, Yassine KOUBAA* and Ahmed TOUMI

*Research Unity of Industrial Process Control (UCPI)
National Engineering School of Sfax (ENIS), B.P.: W 3038 Sfax-Tunisia*

E-mail(s): tarek.aroui@eniso.rnu.tn, yassine.koubaa@enis.rnu.tn,
ahmad.tomi@enis.rnu.tn

Abstract

In this paper, a transient model of the faulty machine is developed. The model is referred to a three phase stator winding, while the rotor has been represented by all the meshes allowing for the representation of various faults. The model is based on coupled magnetic circuit theory by considering that the current in each bar is an independent variable. The model incorporates non-sinusoidal air-gap magneto motive force (MMF) produced by both stator and rotor, therefore it will include all the space harmonics in the machine. Simulations and experimental results were then used to study rotor faults cause-effect relationships in the stator current and the frequency signature.

Keywords

Induction machines; Broken rotor bars and end-rings; Coupled magnetic circuit; Current spectrum.

Introduction

The use of induction motors in today's industry is extensive and the motor can be exposed to different hostile environments, misoperations and manufacturing defects. Internal motor faults (e.g., short circuit of motor leads, interturn short circuits, ground faults, bearing and gearbox failures, broken rotor bar and cracked rotor end-rings), as well as external motor faults (e.g., phase failure, asymmetry of main supply and mechanical overload), are expected to happen sooner or later [4]. Furthermore, the wide variety of environments and conditions

that the motors are exposed to can age, the motor can make it subject to incipient faults. These incipient faults, or gradual deterioration, can lead to motor failure if left undetected.

Early fault detection allows preventative maintenance to be scheduled for machines during scheduled downtime and prevents an extended period of downtime caused by extensive motor failure, improving the overall availability of the motor driven system. With proper system monitoring and fault detection schemes, the costs of maintaining the motors can be greatly reduced, while the availability of these machines can be significantly improved.

Many researchers have focused their attention on incipient fault detection and preventive maintenance in recent years. There are invasive and noninvasive methods for machine fault detection. The noninvasive methods are more preferable than the invasive methods because they are based on easily accessible and inexpensive measurements to diagnose the machine conditions without disintegrating the machine structure.

In order to develop technologies for motor fault detection and diagnosis, it is important to show the proposed theory, schemes, feasibility, and limitations. In the research stage, we require a controllable environment so that we know what types of faults are induced and what types of motor performance are resulted.

The objective of this paper is to develop a model, which is capable to predict the performance of induction machines under rotor failures during transient as well as at steady state.

Induction Machine Modeling

This model follows the coupled magnetic approach by treating the current in each rotor bar as an independent variable. The effect of non-sinusoidal air-gap MMF produced by both the stator and the rotor currents have been incorporated into the model. This is done by use of the winding function approach.

The analysis is based on the following assumptions [9, 11]: Symmetric machine, uniform air-gap, negligible saturation and insulated rotor bar.

The stator comprises of three phase concentric winding. Each of these windings is treated as a separate coil. The cage rotor consists of n bars can be described as n identical and equally spaced rotor loop [1,3,11]. As shown in Figure 1, each loop is formed by two adjacent rotor bars and the connecting portions of the end-rings between them. Hence, the rotor circuit has $n+1$ independent currents as variables. The n rotor loop currents are coupled to each other and to the stator windings through mutual inductances. The end-ring loop does not couple

with the stator windings [7,11], it however couples the rotor currents only through the end leakage inductance and the end-ring resistance.

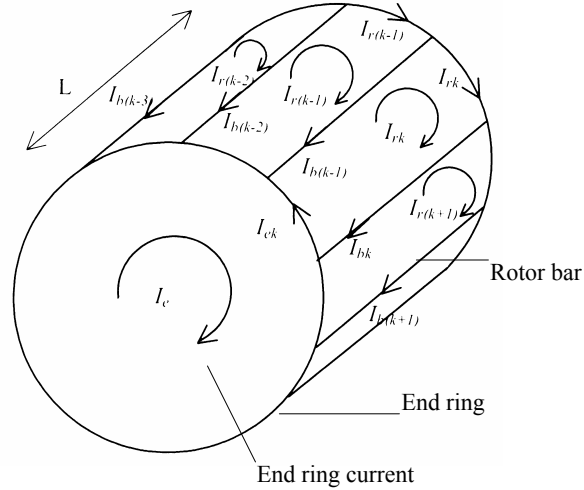


Figure 1. Elementary rotor loops and current definitions

Stator Voltage Equations

The stator equations for the induction machine can be written in vector matrix form as:

$$[\mathbf{V}_s] = [\mathbf{R}_s] [\mathbf{I}_s] + \frac{d}{dt} [\Phi_s] \quad (1)$$

where

$$[\mathbf{V}_s] = \begin{bmatrix} V_{s1} \\ V_{s2} \\ V_{s3} \end{bmatrix}; [\mathbf{I}_s] = \begin{bmatrix} I_{s1} \\ I_{s2} \\ I_{s3} \end{bmatrix}; [\Phi_s] = \begin{bmatrix} \Phi_{s1} \\ \Phi_{s2} \\ \Phi_{s3} \end{bmatrix} \quad (2)$$

and

$$[\Phi_s] = [\mathbf{L}_{ss}] [\mathbf{I}_s] + [\mathbf{L}_{sr}] [\mathbf{I}_r] \quad (3)$$

The matrix $[\mathbf{R}_s]$ is a diagonal 3 by 3 matrix which consists of resistances of each coil.

Due to conservation of energy, the matrix $[\mathbf{L}_{ss}]$ is a symmetric 3 by 3 matrix. The mutual inductance $[\mathbf{L}_{sr}]$ matrix is an 3 by n matrix comprised of the mutual inductances between the stator coils and the rotor loops.

$$[\mathbf{L}_{sr}] = \begin{bmatrix} L_{sr11} & L_{sr12} & \cdots & L_{sr1n} & L_{sr1e} \\ L_{sr21} & L_{sr22} & \cdots & L_{sr2n} & L_{sr2e} \\ L_{sr31} & L_{sr32} & \cdots & L_{sr3n} & L_{sr3e} \end{bmatrix} \quad (4)$$

where L_{srij} is the mutual inductance between the stator phase i ($i = 1, 2$ or 3) and the rotor loop j and L_{srie} the mutual inductance between the stator phase i ($i = 1, 2$ or 3) and the end-ring.

Rotor Voltage Equations

Given the structural symmetry of the rotor, it is convenient to model the cage as identical magnetically coupled circuits. For simplicity, we assume that each loop is defined by two adjacent rotor bars and the connecting portions of the end-rings between them [1, 10].

For the purpose of analysis, each rotor bar and segment of end-ring is substituted by an equivalent circuit representing the resistive and inductive nature of the cage. Such an equivalent circuit is shown in Figure 2.

From Figure 2, the voltage equations for the rotor loops can be written in vector matrix form as:

$$[V_r] = [R_r][I_r] + \frac{d}{dt}[\Phi_r] \tag{5}$$

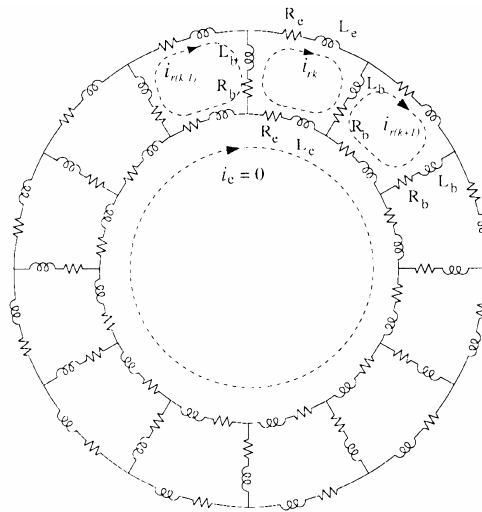


Figure 2. Rotor cage equivalent circuit showing rotor loop currents and circulating end ring current.

Where

$$[V_r] = [V_{r1} V_{r2} \dots V_m V_{re}]^t \tag{6}$$

In case of a cage rotor, the rotor end ring voltage is $V_{re}=0$, and the rotor loop voltages are $V_{rk}=0, k=1,2\dots n$.

The loop equation for k th rotor circuit is:

$$V_{rk} = 0 = 2(R_b + R_e) I_{rk} - R_b I_{r(k-1)} - R_b I_{r(k+1)} - R_e I_e + \frac{d\Phi_{rk}}{dt} \quad (7)$$

The voltage equation for the end-ring is:

$$V_{re} = 0 = -R_e I_{r1} - R_e I_{r2} - \dots - R_e I_{rn} + n R_e I_{re} + \frac{d\Phi_{rk}}{dt} \quad (8)$$

where R_b is the rotor bar resistance and R_e is the end-ring segment resistance.

Since each loop is assumed to be identical, the equation (7) is valid for every loop. Therefore the resistance matrix $[R_r]$ is a symmetric $(n+1)$ by $(n+1)$ matrix given by:

$$[R_r] = \begin{bmatrix} 2(R_b + R_e) & -R_b & 0 & \vdots & 0 & -R_b & -R_e \\ -R_b & 2(R_b + R_e) & -R_b & \vdots & 0 & 0 & -R_e \\ \vdots & \vdots & \vdots & \vdots & \vdots & \vdots & \vdots \\ \vdots & \vdots & \vdots & \vdots & \vdots & \vdots & \vdots \\ 0 & 0 & 0 & \vdots & 2(R_b + R_e) & -R_b & -R_e \\ -R_b & 0 & 0 & \vdots & -R_b & 2(R_b + R_e) & -R_e \\ -R_e & -R_e & -R_e & \vdots & -R_e & -R_e & nR_e \end{bmatrix} \quad (9)$$

In relation (5), the rotor flux can be written as:

$$[\Phi_r] = [L_{rs}][I_s] + [L_{rr}][I_r] \quad (10)$$

Due of the structural symmetry of the rotor, $[L_{rr}]$ can be written in matrix form (11), where L_{kk} is the self inductance of the k th rotor loop, L_b is the rotor bar leakage inductance, L_e is the rotor end-ring leakage inductance and L_{ki} is the mutual inductance between two rotor loop.

$$\begin{aligned}
 & [L_{rr}] = \\
 & \begin{bmatrix}
 L_{11} + 2(L_b + L_e) & L_{12} - L_b & L_{13} & \cdots & L_{1(n-1)} & L_{1n} - L_b & -L_e \\
 L_{21} - L_b & L_{22} + 2(L_b + L_e) & L_{23} - L_b & \cdots & L_{2(n-1)} & L_{2(n-1)} & -L_e \\
 \vdots & \vdots & \vdots & \cdots & \vdots & \vdots & \vdots \\
 \vdots & \vdots & \vdots & \cdots & \vdots & \vdots & \vdots \\
 L_{(n-1)1} & L_{(n-1)2} & L_{(n-1)3} & \cdots & L_{(n-1)(n-1)} + 2(L_b + L_e) & L_{(n-1)n} - L_b & -L_e \\
 L_{n1} - L_b & L_{n2} & L_{n3} & \cdots & L_{n(n-1)} - L_b & L_{nn} + 2(L_b + L_e) & -L_e \\
 -L_e & -L_e & -L_e & \cdots & -L_e & -L_e & nL_e
 \end{bmatrix} \\
 & \hspace{20em} (11)
 \end{aligned}$$

Calculation of Torque

The mechanical equation of the machine is [7]:

$$C_{em} - C_r = J \frac{d\Omega_m}{dt} \quad (12)$$

where C_{em} is the electromagnetic torque, C_r is the load torque, J is the inertia of the rotor and Ω_m is the mechanical speed.

with

$$\Omega_m = \frac{1}{p} \frac{d\theta}{dt} \quad (13)$$

where θ is the angular position of the rotor and p denotes the number of motor pole pairs.

The electromagnetic torque is given by the following equation [11]:

$$C_{em} = P I_s^t \left\{ \frac{d}{d\theta} [L_{sr}] \right\} I_r \quad (14)$$

Calculation of Inductances

It is apparent that the calculation of all the machine inductances as defined by the inductances matrices in the previous section is the key to the successful simulation of an induction machine.

The model must take into account the geometric construction of the machine and then include the entire space harmonic.

These machine inductances are conveniently calculated by means of winding functions. This method assumes no symmetry in the placement of any motor coil in the slots.

According to winding function theory, the mutual inductance between two windings i and j in any electric machine can be computed by the following equation [6, 10, 12]:

$$L_{ij}(\theta) = \frac{\mu_0 l r}{g} \int_0^{2\pi} \varepsilon_i(\theta, \phi) \varepsilon_j(\theta, \phi) d\phi \quad (15)$$

where $\mu_0 = 4\pi \cdot 10^{-7}$ H/m, g is the air gap, θ is the angular rotor position, r is the average radius of the air gap, l is the active length of the motor, ϕ is a particular point along the air gap and $\varepsilon_i(\theta, \phi)$ is called the winding function and represents the magneto motive force (MMF) distribution along the air gap for a unit current flowing in winding i .

For simulation purposes a three phase, 4Kw, 50hz, 4 pole, 380/220V squirrel-cage induction motor will be treated in this paper. The machine has a stator comprises of three phase concentric winding with 36 slots, 28 rotor bars and two coils per phase. Figure4 shows the MMF distribution produced by 1A of current through the stator phase "1". Note that both stator phases, "2" and "3", produce a similar MMF distribution but shifted by $\pi/3$ and $2\pi/3$.

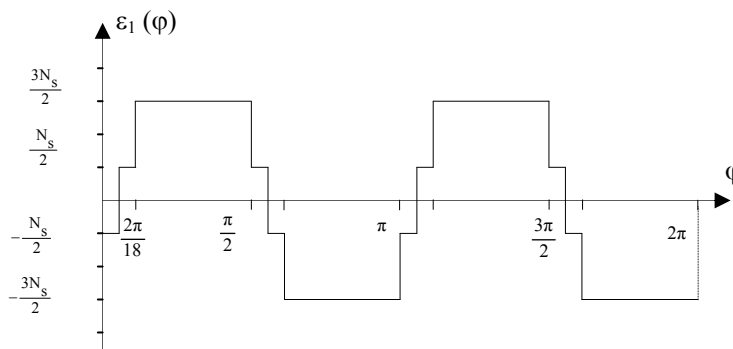


Figure 4. MMF distribution of the stator phase "1"

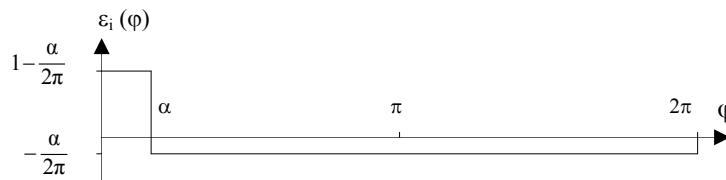


Figure 5. MMF distribution of the rotor loop "1"

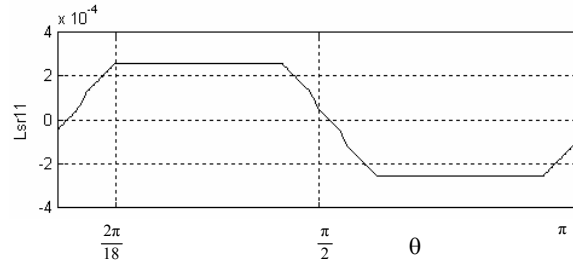


Figure 6. Mutual inductance between the stator phase "1" and rotor loop "1"

The MMF distribution produced by 1A of current through a rotor loop can only take two values depending on whether we are inside or outside the loop. The angle between two adjacent rotor bars is $\alpha = \frac{\pi}{14}$, the MMF distribution produced by 1A of current through the first rotor loop, is shown in Figure 5.

The mutual inductance between stator and rotor branches will be a function of the rotor position angle θ . Figure 6 gives the mutual inductance ($L_{sr11}(\theta)$) between the stator phase "1" and the rotor loop "1". Note that the mutual inductance between the phase "2" and the rotor loop "1" is $L_{sr11}(\theta)$ but shifted to the right by 6γ where γ is the angle between two stator slots. Mutual inductance between the phase "1" and the rotor loop "2" is $L_{sr11}(\theta)$ but shifted to the left by α where α is the angle between two rotor bars.

Simulation Results

To validate the proposed model, a functional schema of the induction machine was developed on the Matlab-Simulink platform.

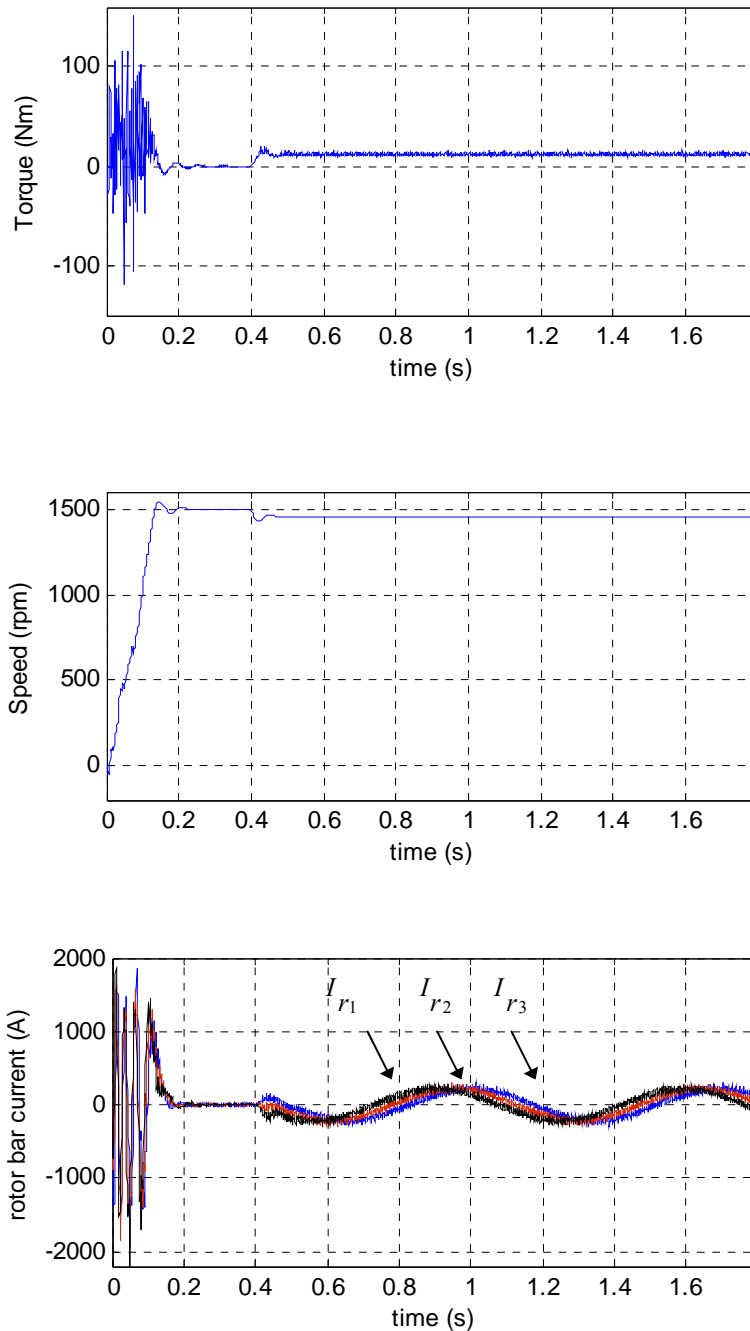
Figure 7 Shows the instantaneous electromagnetic torque, speed, rotor bar current and the phase current of the machine during a start up with a balanced sinusoidal voltage supply followed by the application of a load ($C_r = 11\text{Nm}$) at instant $t=0.8\text{s}$.

Modelling Rotor Bars and End-Ring Faults

Rotor fault have been simulated by including proper relationships between the rotors current variables and reducing the coupling inductance matrix. If the bar between loop k and loop $(k+1)$ is an open circuited, then we require $I_{rk} = I_{r(k+1)}$ which means that the current is I_{rk} flowing in a double width loop as shown in Figure 8.

This condition is impressed on the inductance matrix $[L_{rr}]$ by adding the column relating to I_{rk} , meaning the column k to that relating to $I_{r(k+1)}$ which is the column $k+1$. The same relationship is applied to the corresponding rows. Similar measures are taken for the resistance matrix $[R_r]$. The same process is done on the column of mutual inductance $[L_{sr}]$.

Further open circuited bars are incorporated by repeating the above mentioned reduction process, as required [1].



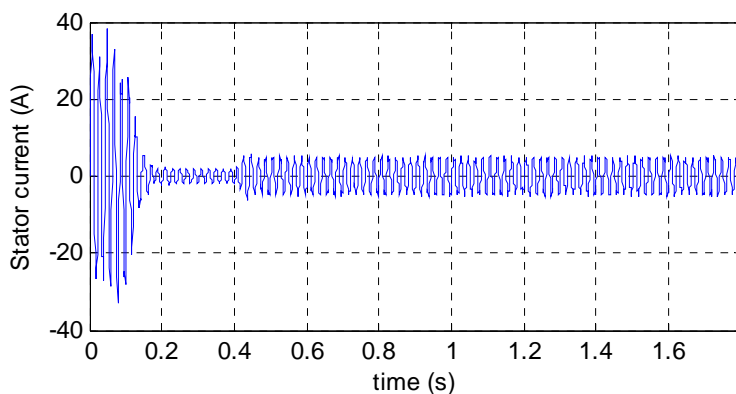


Figure 7. Torque, speed, rotor currents and stator current in phase "1" (top to bottom). Normal machine

For the broken end-ring in the section of the k th rotor loop the corresponding loop current is zero as is presented in Figure 9. This situation occurs when $I_{rk} = I_{re}$ [1].

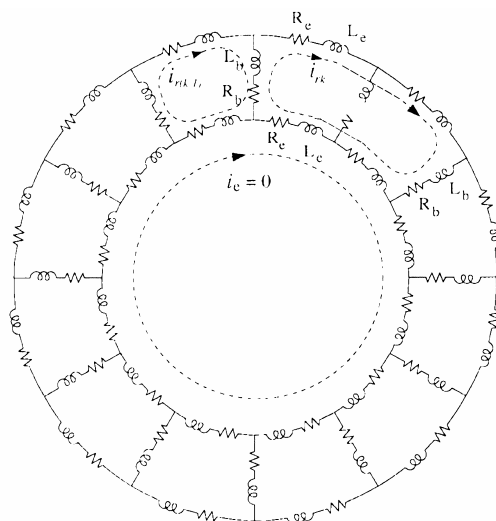


Figure 8. Representation of broken bar

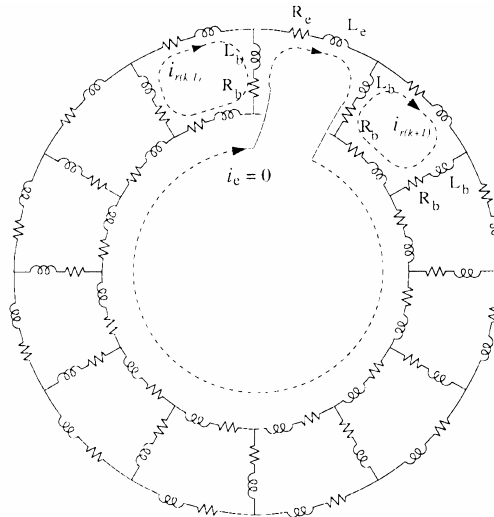
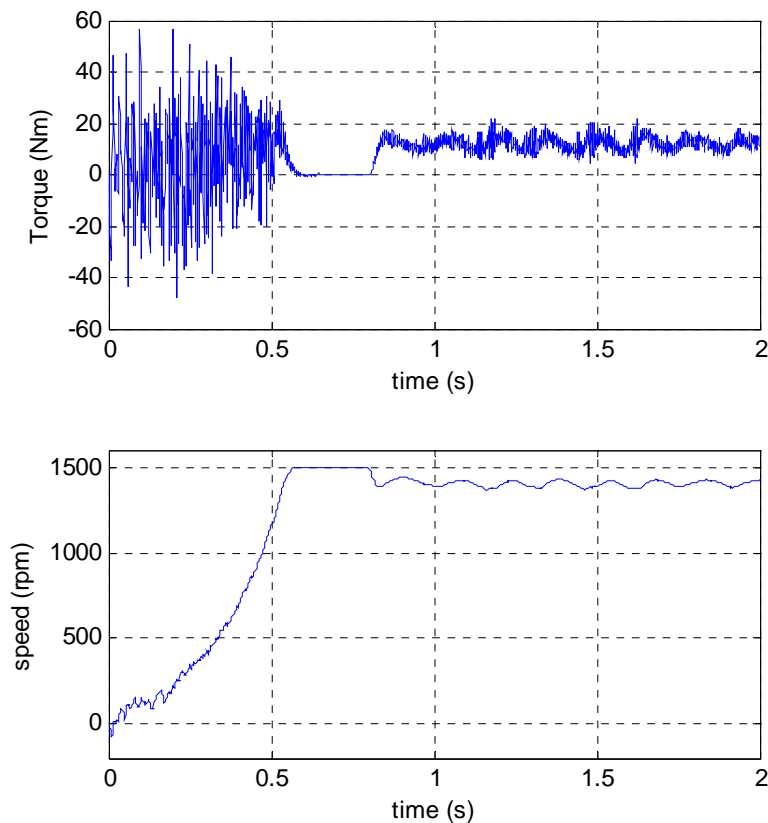


Figure 9. Representation of broken end-ring

Simulation Results

Figure 10 Shows the instantaneous electromagnetic torque, speed and the phase current of the machine with four broken rotor bars and one end-ring, during a start up with a balanced sinusoidal voltage supply followed by the application of a load ($C_r = 11\text{Nm}$) at instant $t=0.8\text{s}$.



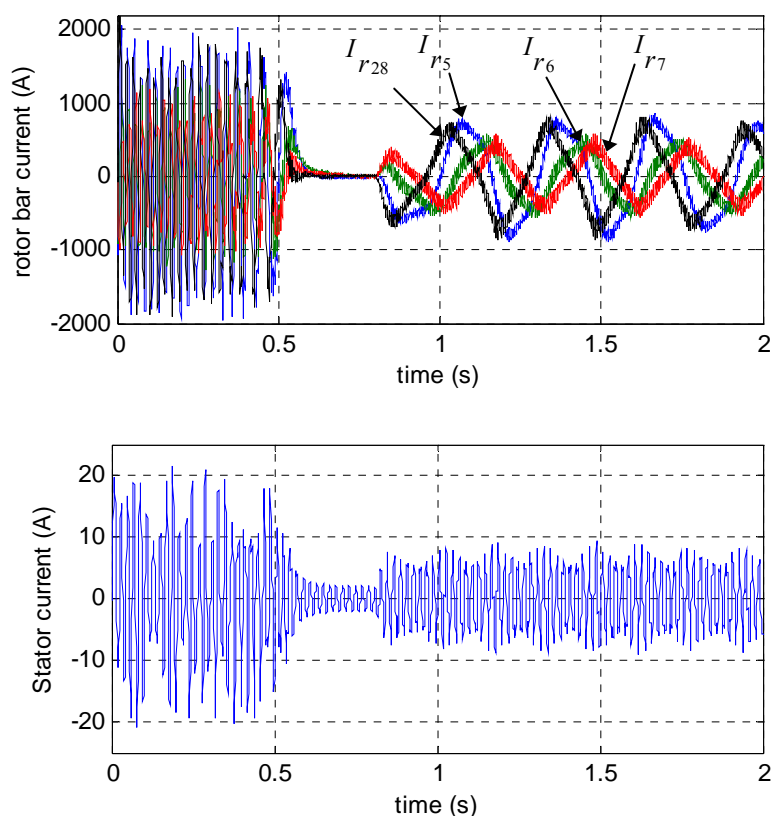


Figure 10. Torque, speed, rotor currents and stator current in phase "1" (top to bottom). Machine with four broken rotor bars and one end-ring

We can easily see that the effect of four broken rotor bars and one end-ring is very important. (e.g., the acceleration time under rotor asymmetry is larger than under healthy machine).

Analysis of Steady State Operation

The stator current signal at steady state for the loaded machine is transformed by the Fast Fourier Transform (FFT) into signal in the frequency domain to generate the power spectral density (PSD). The spectrum generated by this transformation includes only the magnitude information about each frequency component, which can be analyzed and processed easier than signal in the time domain.

Spectrum Analysis in the Bandwidth [25Hz-75Hz]

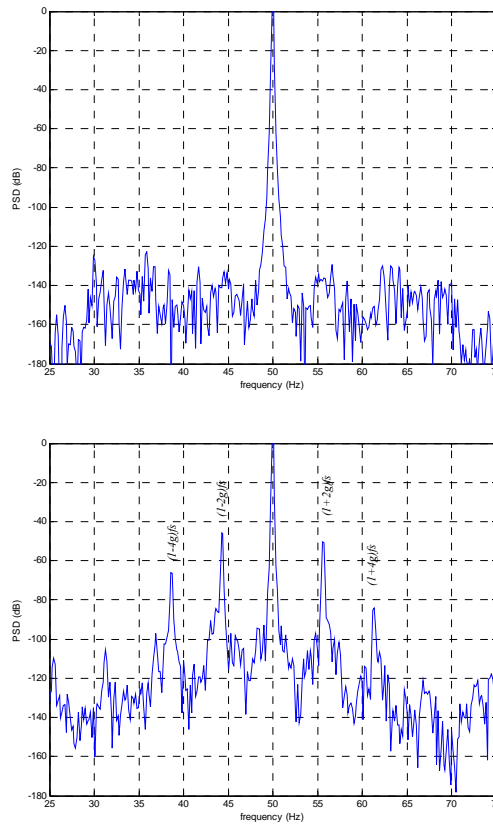


Figure 11. Simulated stator current spectrum for healthy machine and for the case of four broken rotor bars and one end-ring (top to bottom)

Figure 11 reports stator current spectrum around fundamental for a normal machine and a machine with four broken bars and one broken end-ring. We can see that rotor anomalies induce some harmonic components, given by [1,8]:

$$f_{bc} = (1 \pm 2ks)f_s, k = 1, 2, 3, \dots \tag{16}$$

Spectrum Analysis in the Bandwidth [100Hz-1000Hz]

There are other spectral components that can be observed in the stator line current due to broken rotor bar fault. The equation describing these frequency components is given by Benbouzid [2] and Nandy [8]

$$f_{hbc}^{\pm} = \left[\left(\frac{k}{p} \right) (1-s) \pm s \right] f_s \tag{17}$$

where, f_{hbc}^{\pm} are detectable broken bar frequencies; $\frac{k}{p}=3, 5, 7, 9, 11, 13, \dots$

Figure 12 shows the simulated plot of the stator currents spectrum affected by the frequency components f_{hbc}^{\pm} around 5th and 7th time harmonic with rotor failures.

By analyzing a zoom around the 5th time harmonic (Figure 13), we can visualize the presence of the principal components f_{hbc}^{\pm} . We notice the presence of additional frequency components which are spaced by $2sf_s$. This can be verified on space harmonic 7, 11, 13 ...

Then, it is necessary to complete equation (17) to take into consideration these harmonics because they are indicative of failure presence in the rotor cage. The new equation will be:

$$f_{hbc} = \left[\left(\frac{k}{p} \right) (1-s) \pm (1+2\beta)s \right] f_s \quad (18)$$

where, f_{hbc} is detectable broken bar frequencies; $\frac{k}{p}=3, 5, 7, 9, 11, 13, \dots$ And $\beta = 0, 1, 2, 3, \dots$

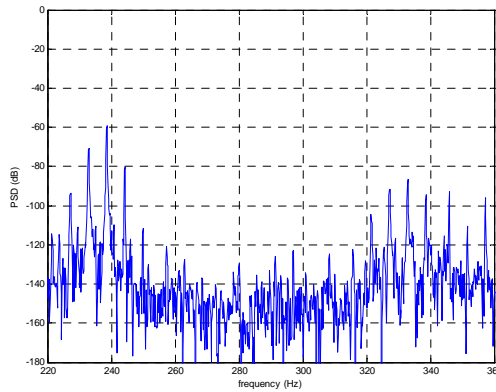


Figure12. Simulated stator current spectrum for faulty machine around the 5th and 7th time harmonic

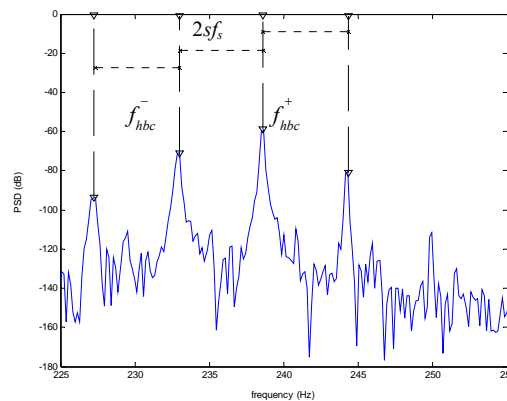


Figure13. Simulated stator current spectrum for faulty machine around the 5th time harmonic

Experimental Setup and Results

The characteristics of the 3 phase induction motor used in our experiment are listed in Table1. The needed load of the induction motor was established by connecting the test motor to an eddy current brake via a flexible coupling (Figure14). In order to allow tests to be performed at different load levels, the brake DC supply current is controllable.

A current Hall Effect sensor was placed in one of the line current cables. The stator current was sampled with a 4 KHz rate and interfaced to a pentium PC by an ARCOM acquisition board.

The motor was tested with the healthy rotor and a faulty rotor with two broken bars. The bars were broken by drilling holes through them.

Table 1. Induction motor Characteristics used in the experiment

<i>Description</i>	<i>Value</i>
Power	5.5 kW
Input Voltage	220/380 V
Full load current	20.6/11.9A
Supply frequency	50 Hz
Number of poles	2
Number of rotor slots	28
Number of stator slots	36
Full load speed	2875 rpm



Figure 14. View of the experimental setup

As predicted by simulation, Figure15 and Figure16 show the experimental results with healthy and faulty machine around fundamental. We can see the amplitude of the sidebands components f_{bc} according to equation (16) in the faulty machine current increase over their counterpart in the case of the healthy machine.

Experimental results show significant changes around the 5th time harmonic (Figure17). According to equation (18), space harmonic spaced by $2sf_s$ can be clearly seen.

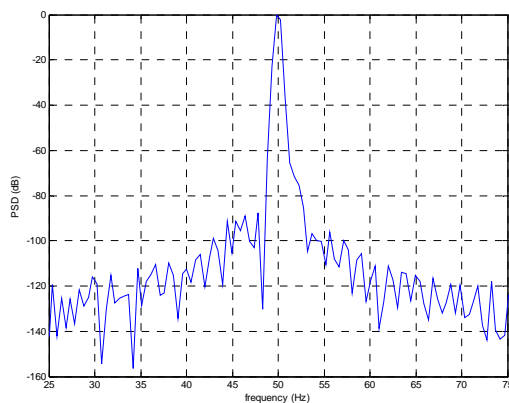


Figure15. Experimental plots of stator current spectrum around fundamental of the healthy machine

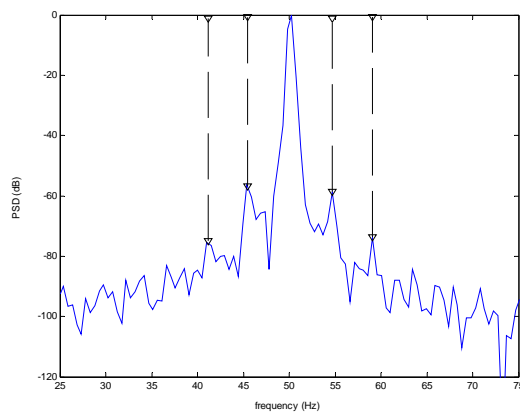


Figure16. Experimental plots of stator current spectrum around fundamental of the faulty machine with two broken bars

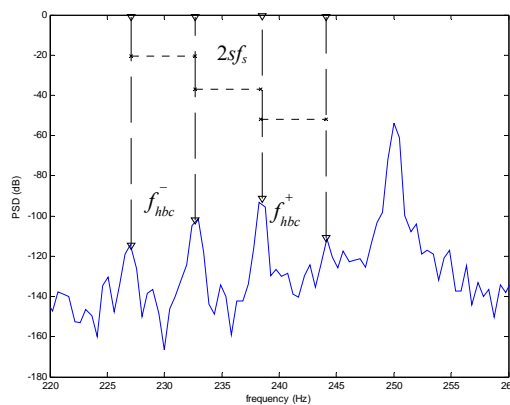


Figure17. Experimental plots of stator current spectrum around 5th time harmonic of the faulty machine with two broken bars

Conclusion

A detailed model of a squirrel-cage induction machine has been developed. In order to simulate incipient broken rotor bar and end-ring fault, the machine was modeled as a group of coupled magnetic circuits by considering the current in each rotor bar as an independent variable. The model can simulate the performance of induction machines during transient as well as at steady state, including the effect of rotor faults. Simulation and experimental results were then used to identify low and high frequency spectral components created by rotor anomalies in the stator current spectrum.

Acknowledgement

The authors would like to thank SITEX Company who finances this work. They also wish to express their deep appreciation for the support rendered by the electrical department members

References

1. Ah-Jaco A., *Modélisation des moteurs asynchrones triphasés en régime Transitoire avec saturation et harmoniques d'espace. Application au diagnostic*, thèse de doctorat de l'université de Lyon juillet 1997.
2. M.E.H. Benbouzid, *A review of induction Motors signature analysis as a medium for faults detection*, IEEE Transaction on Industrial Electronics, vol. 47, N° 5, pp 984-993, October 2000.
3. Casimir R. E. Bouteleux, Yahoui H., G. Clerc , Henao H., C. Delmotte, Capolino G.-A., Rostaing G., Rognon J.-P., Foulon E., Loron L., Didier G., Razik H., Houdouin G., Barakat G., Dakyo B., Bachir S., Tnani S., Champenois G., Trigeassou J.C., Devanneaux V., DagueB. and Faucher J., *Comparaison de plusieurs méthodes de modélisation et de diagnostic de la machine asynchrone en présence de défauts*, Proceedings of EF'2003 Electrotechnique du futur, 9 et 10 décembre 2003, Supélec.
4. M. Y. Chow, *Methodologies of using neural network and fuzzy logic technologies for motor incipient fault detection*, World Scientific Publishing Co. Pte. Ltd, Singapore, 1997.
5. Filippetti F., Franceschini G., Tassoni C. and Vas,P., *AI techniques in induction machines diagnosis including the speed ripple effect*, IEEE Trans. Indus. Appli. Vol.34, n°1, pp.98-108, 1998.
6. Luo X., Liao Y., Toliyat H.A., El-Antably A. and Lipo T.A., *Multiple coupled circuit modeling of induction machines*, IEEE Transaction on Industry applications, vol. 31, N° 2, pp 311-318, March/April 1995.
7. Munoz A.R. and Lipo T.A., *Complex vector model of the squirrel-cage induction machine including instantaneous rotor bar currents*, IEEE-IAP, vol. 35, N°6, 1999

8. Nandi S. and Toliyat H.A., *Condition monitoring and fault diagnosis of electrical machines—A review*, in Conf. Rec. IEEE-IAS Annu. Meeting, vol. 1, Phoenix, AZ, pp. 197–204. 1999
9. Razik H. and Gaëtan D., *Sur la détection d'un défaut au rotor des moteurs asynchrones*, La revue 3EI n° 27, Décembre 2001
10. Toliyat H.A., Lipo T.A., and White J.C., *Analysis of a concentrated winding induction machine for adjustable speed drive application part I (Motor analysis)*, IEEE Transaction on Energy Conversion, vol. 6, N° 4, pp 679-684, Dec 1991.
11. Toliyat H.A. and Lipo T.A., *Transient analysis of cage induction machines under stator, rotor bar and end-ring faults*, IEEE Transaction on Energy Conversion, vol. 10, N° 2, pp 241-247, June 1995.
12. Al-Nuaim N.A. and Toliyat H.A., *A novel method for modeling dynamic air-gap eccentricity in synchronous machines based on modified winding function theory*, IEEE Transaction on Energy Conversion, vol. 13, N° 2, pp 156-162, June 1998.